Measured Magnetic-Field Evolution and Instabilities in Laser-Produced Plasmas

The stability of plasmas with magnetic (B) fields is a critical issue for basic and applied plasma physics; instabilities may lead to important (and sometimes catastrophic) changes in plasma dynamics.[1] Intensive studies of various instabilities have been conducted for a wide range of plasmas and fields, particularly in the areas of magnetic-confinement plasmas[2] and space physics.[3] In laser-produced, high-energy-density (HED) laboratory plasmas, however, experimental studies of B-field–related instabilities have been rare because of limitations in experimental methods. In particular, resistive instabilities, a large category of macroscopic instabilities, have not been observed previously in this regime, partly because they are not important in the hot, low-resistivity plasmas usually studied.[4]

In the experiments described here, monoenergetic proton radiography was used for the first time to study the time evolution of the B-field structure that is generated by the interaction of a long-pulse, low-intensity laser beam with plasma. This work focuses on the qualitative and quantitative study of the physics involved in field evolution and instabilities over a time interval much longer than the laser pulse length, and B fields generated by laser–plasma interactions experience a tremendous dynamic range of plasma conditions. While the laser is on, we study field generation (via $\nabla n_e \times \nabla T_e$),[4–6] growth, and the balance between energy input and losses. After the laser turns off, laser absorption at the critical surface ends and the plasma cools down. Fields start to decay and dissipate, and field diffusion [$\nabla \times (D_m \nabla \times \mathbf{B})$, where D_m is the magnetic diffusion coefficient[4–6]] becomes increasingly important relative to convection [$\nabla \times (\mathbf{v} \times \mathbf{B})$, where $\mathbf{v}$ is the plasma fluid velocity[4–6]] as the cooling plasma becomes more resistive. At these later times, physical processes associated with resistivity tend to dominate over fluid effects, particularly around the bubble edge where the plasma β values, a ratio of thermal to field energies, are smaller than one.

The approach described here allows us to make a direct comparison of proton images recorded at different times, to measure field evolution, to address different physics processes in different regimes, and, most importantly, to identify resistivity-induced instabilities. Most previous work in this field has involved high-intensity, short-pulse lasers[7] or long-pulse lasers with limited diagnostic measurements.[8] Preliminary measurements we made while a laser beam was on have recently been published,[9] but the work described here uniquely covers times extending well past the end of the laser pulse and reveals important new phenomena that were not previously seen and are not predicted by two-dimenstional (2-D) simulation codes. The first observation of repeatable, asymmetric structure around the plasma bubbles at late times provides important insights into pressure-driven magnetohydrodynamic (MHD) instabilities in resistive plasmas,[2] while the first observation of nonrepeatable chaotic structure within the plasma bubble provides likely evidence of the electron thermal instability.[10] Simulations[11] of these experiments with the 2-D hydrodynamic code *LASNEX*[12,13] and hybrid PIC code *LSP*[14] have been performed; they are qualitatively useful for interpreting the observations but diverge from our measurements (particularly after the laser beam is off).

The setup of the experiments performed on OMEGA[15] is illustrated schematically in Fig. 109.21. B fields were generated through laser–plasma interactions on a plastic (CH) foil by a single laser beam (henceforth called the *interaction beam*) with a wavelength of 0.351 μm, incident 23° from the normal

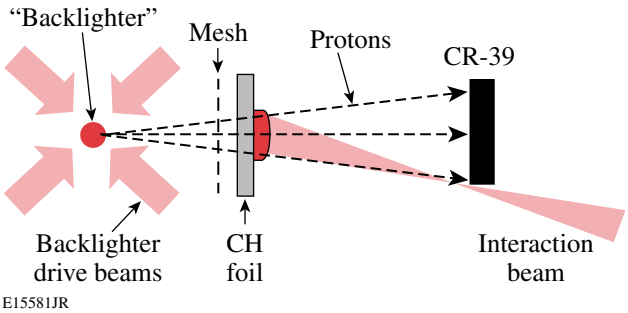

Figure 109.21
Schematic illustration of the experimental setup for face-on proton radiography. Distances from the backlighter are 1.3 cm for the mesh, 1.5 cm for the CH foil (5 μm thick), and 30 cm for the CR-39 detector.

direction. The laser had a 1-ns-long square pulse, an energy of ~500 J, and a spot diameter of 800 μm determined by phase plate SG4 (defined as 95% energy deposition),[16] resulting in a laser intensity of the order of 10^{14} W/cm^2.

The fields were studied with monoenergetic proton radiography, using a backlighter that produced protons at the two discrete energies of 14.7 MeV and 3 MeV (fusion products of the nuclear reactions D + ^{3}He → α + p and D + D → T + p, respectively, generated from D^{3}He-filled, exploding-pusher implosions driven by 20 OMEGA laser beams).[9,17] The duration of the backlighter was ~150 ps, and the timing of the interaction laser was adjusted in different experiments so the arrival of the backlighter protons at the foil would occur with different delays after the laser interaction beam was turned on. Separate radiographs made with the two proton energies were recorded simultaneously using stacked CR-39 detectors arranged with filters so that only one detector was sensitive to each energy.[18] A nickel mesh (60 μm thick with a 150-μm hole-to-hole spacing) was used to divide the backlighter protons into discrete beamlets, and, for the 14.7-MeV protons, the deflections of these beamlets due to fields in laser-induced plasmas on CH foils were measured in the images.

Images made with these monoenergetic-proton backlighters have distinct advantages over images made with broadband sources: measured image dimensions and proton beamlets deflections provide unambiguous quantitative information about fields; detectors can be optimized; and the backlighter is isotropic (simultaneous measurements can be made in multiple directions[17] and the source can be monitored at any angle).

Face-on images made with D^{3}He protons are shown in Fig. 109.22(a). The laser timing was adjusted so that these 14.7-MeV protons arrived at the foil at various times between 0.3 ns and 3 ns after the laser interaction beam was turned on. Since the interaction-beam pulse was 1 ns square with ~0.1-ns rise and decay times, the data covered two time intervals: 0.3 to 0.9 ns when the laser was on, and 1.2 to 3 ns when the laser was off. Each image shows how the proton beamlets are deflected while passing through the magnetic field that formed around the plasma bubble generated by the interaction beam, as described previously.[9,11,17]

While the interaction beam is on, each image has a sharp circular ring where beamlets pile up after passing through the edges of the plasma bubble where the maximum B fields were generated. The deflection of each beamlet is proportional to the integral $\left| \int \mathbf{B} \times d\ell \right|$ (where $d\ell$ is the differential pathlength along the proton trajectory), and this integral is highest at the edge of the bubble. Beamlets in the center of each image undergo less radial deflection, indicating that the integral $\left| \int \mathbf{B} \times d\ell \right|$ is much smaller there. These features are well reproduced by *LASNEX + LSP* simulations, as shown in Fig. 109.22(b) (0.3 to 0.9 ns). Figure 109.23(a) shows the

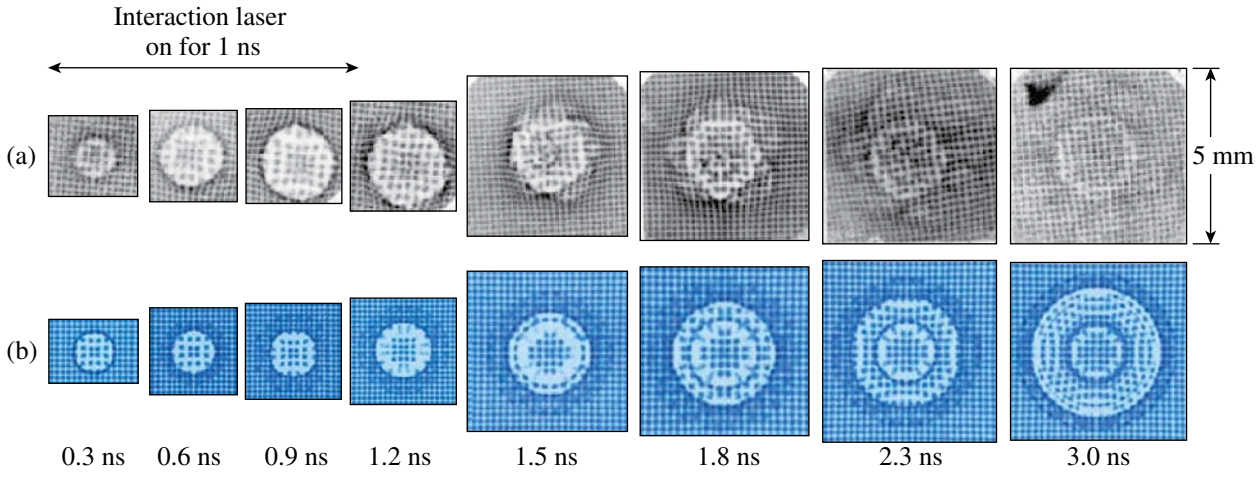

Figure 109.22
(a) Measured face-on D^{3}He proton images showing the spatial structure and temporal evolution of the B fields generated by laser–plasma interactions. Each image is labeled by the time interval between the arrival of the interaction beam at the foil and the arrival of the imaging protons. The images illustrate the transition from 2-D symmetric expansion of magnetic fields, during a 1-ns laser illumination, to a more-asymmetric 3-D expansion after the laser turned off and the plasma cooled and became more resistive; this asymmetry is conjectured to be driven by a resistive MHD interchange instability. (b) Images simulated by *LASNEX + LSP* for the conditions that produced the experimental images shown in (a).

magnetic field predicted in these simulations in a plane perpendicular to the foil at 0.6 ns. The protons would travel from right to left in the plane of this field map, and the maximum line integrals would be at the edges.

At times after the laser beam is off, the simulations do not track the data as well. As shown in Fig. 109.22(b) (1.5 to 3 ns), simulations predict that the proton images have a double ring structure. The outer ring comes from the outer edge of the plasma bubble where large ∇T_e occurred; the inner ring comes from the toroidal magnetic field at the edge of the hole burned into the plastic by the interaction laser, as seen in Fig. 109.23(b) for 1.5 ns. Figure 109.23(b) shows that the simulations also predict a second plasma bubble with a surface B field on the rear face of the foil after the laser has completely burned through; the direction of this field is reversed relative to the field on the front of the foil, but the simulated images show no major feature associated with this field because it is relatively weak.

At 2.3 ns in Fig. 109.22, the data and simulation are generally similar to each other. They each have an inner ring that corresponds to the burnthrough field, as described above, though it is a little smaller in the simulation than in the data. They each show a boundary farther out that corresponds to the outer surface of the bubble, but in the data it is strikingly asymmetric while in the simulation it is round because the code is limited to a 2-D structure.

We believe this is the first direct observation of the pressure-driven, resistive MHD interchange instability in laser-produced HED plasmas at the interface between the bubble and field. This instability, which involves the interchange of field between the inside and outside of the bubble surface, occurs when the plasma is resistive and there is unfavorable field curvature ($\boldsymbol{\kappa} \cdot \nabla p > 0$, where $\boldsymbol{\kappa} = \mathbf{B} \cdot \nabla \mathbf{B}/B^2$ is the field-line curvature and ∇p is the pressure gradient).[2] It makes sense that the instability occurs only after the laser is off, when the cooling plasma becomes more resistive.

There are strong similarities in the angular structure of this region from one image to the next (five to ten cycles over the 360° around the bubble), in spite of the fact that the images are from different shots. It seems that once the power input from the laser disappears, the plasma bubble quickly becomes asymmetric, but something systematic must be seeding the asymmetry. The physics behind this process is conjectured to be highly localized resonance absorption of linearly polarized laser light caused by obliquely incident light (23° from the normal) in an inhomogeneous ($\nabla n_e \neq 0$) plasma.[19] This phenomenon merits future experimental and theoretical investigation.

Another type of instability is apparent during the interval from 1.5 to 2.3 ns, where the distributions of beamlets near the image centers have some chaotic structure. The structures are quite different in each of the three images in this time interval, and since these images are from different shots, it would appear that the structure is random. We note that our earlier work[9] showed that a similar chaotic structure would occur if the laser was on and if no laser phase plates were used; phase plates either prevented the chaotic structure from forming as long as the laser was on or reduced its amplitude sufficiently that it was not visible until it had a chance to grow over a longer time

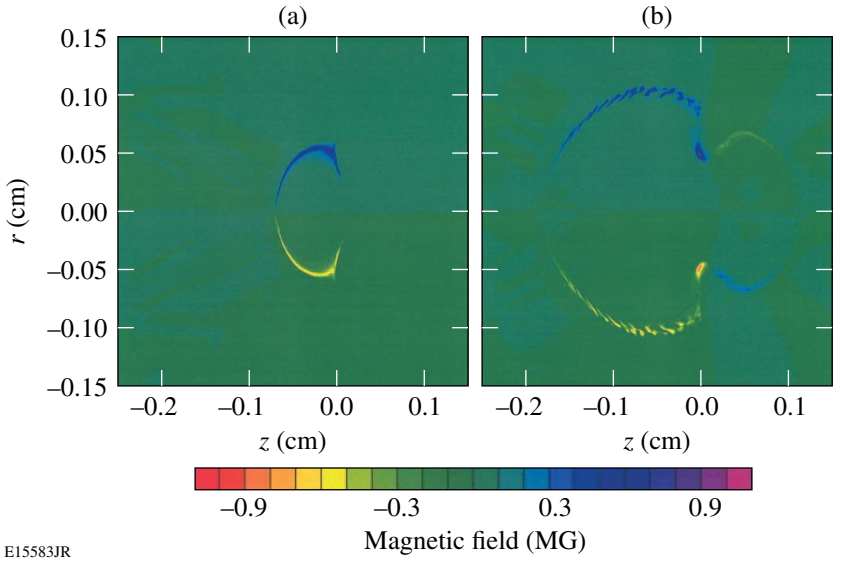

Figure 109.23
Time evolution of *LASNEX*-simulated *B*-field strength on a cross section of the plasma bubble in a plane perpendicular to the foil at (a) ~0.6 ns, when the laser was on, and (b) ~1.5 ns, when the laser was off. In each case, the horizontal coordinate z is the distance from the foil (assuming the laser is incident from the left), and the vertical coordinate r is the distance from the central axis of the plasma bubble. When the laser is on, strong fields occur near the edge of the plasma bubble. After the laser pulse, strong fields also appear near the edge of the hole burned into the foil by the laser and weaker fields (with the opposite direction) appear on the backside of the foil.

period (possibly due to the electron thermal instability when the plasma cools and becomes more resistive, driven by heat flow and leading to a random filamentary structure of n_e and T_e, as well as B fields[10]). The phase plates presumably result in a more-uniform temperature profile and a reduced medium-scale random structure associated with localized regions of strong $\nabla n_e \times \nabla T_e$ (Refs. 9 and 16).

Similar features are seen as late as our last image at 3 ns, although by this time the field strengths have diminished so that the amplitudes of all beamlet displacements are small. Although both simulation and experiment show a continued expansion of the plasma bubble at late times, leading to convective losses, the beamlet displacements in the data are much smaller than those in the simulation, indicating that fields have dissipated much more quickly than predicted. However, since the data reveal a 3-D structure after the laser is off, we have to realize that 2-D computer codes simply cannot model this time interval (although they are still useful for aiding qualitative interpretation of the images, particularly the role of the burnthrough hole in producing a static pattern in the images). Experimental measurements such as those shown here are therefore doubly important since they directly reveal previously unpredicted physical phenomena and also provide invaluable information for benchmarking true 3-D code development in the future.

Quantitative conclusions can be drawn from the images by measuring the sizes of features in the images and the displacements ξ of individual beamlet positions in the images. The displacements ξ of individual beamlet positions in the images result from the Lorenz force $\left| \int \mathbf{B} \times d\ell \right|$ and represent not lateral displacements at the foils but angular deflections from interactions with fields near the foil leading to lateral displacement at the detector. The actual bubble size is thus not determined directly by the apparent size in the image because the image of the bubble is magnified by radial beamlet displacements. The position of the actual bubble edge is inferred by determining the locations that the beamlets in the pileup region would have had in the image without displacement. The result of this analysis is shown in Fig. 109.24(a), where the radius at late times (when the bubble is asymmetric) represents an angular average. We see that the bubble radius grows linearly while the laser is on and then continues to expand after the laser is off. In addition to the radii of the plasma bubble, Fig. 109.24(a) also shows the radius of the burnthrough holes. Once the laser is off, this radius changes very little.

The maximum displacement ξ in each image represents the maximum value of $\left| \int \mathbf{B} \times d\ell \right|$; the values from the images of Fig. 109.22(a) are plotted in Fig. 109.24(b). The maximum value of this integral occurs at the end of the laser pulse, and it decays thereafter; the value predicted by *LASNEX* does not decay as fast. We note that while the laser is on, this maximum occurs at the outside of the plasma bubble, but after the laser is off, the maximum occurs at the edge of the burnthrough hole.

In summary, we have measured the spatial structure and temporal evolution of magnetic fields generated by laser–plasma interactions for the first time over a time interval that is long compared to the laser pulse duration, using monoenergetic proton radiography. Our experiments demonstrated that while a long-pulse, low-intensity laser beam illuminates a plastic foil, a hemispherical plasma bubble forms and grows linearly, surrounded by a symmetric, toroidal B field. After the laser pulse turns off, the bubble continues to expand, but field strengths decay and field structure around the bubble edge becomes asymmetric due, presumably, to the resistive MHD interchange instability. A significant part of that asymmetric structure is repeatable in different experiments, indicating that the asymmetry must have been seeded by some aspect of the experiment, like resonance absorption of obliquely incident, linearly polar-

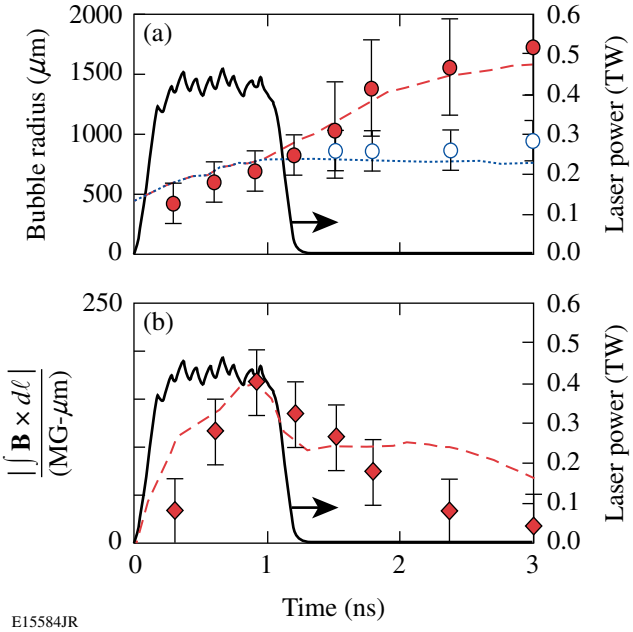

Figure 109.24
(a) Evolution of sizes at the foil, inferred from the images, for the plasma bubble radius (solid circles) and the burnthrough hole (open circles), compared with simulations (dashed and dotted lines, respectively). (b) Evolution of the maximum measured value of $\left| \int \mathbf{B} \times d\ell \right|$ (diamonds), compared with *LASNEX* simulations (dashed line). The solid lines in both (a) and (b) represent the 1-ns OMEGA laser pulse.

ized laser light by an inhomogeneous plasma. Nonrepeatable chaotic structure forms at the center of the plasma bubble after the laser is off, possibly due to a resistivity-induced electron thermal instability. *LASNEX + LSP* simulations agree fairly well with data while the interaction laser is on, aiding the interpretation of the measured images, but the 2-D limitation of these simulations prevents them from predicting some large 3-D structures that develop after the laser is off.

ACKNOWLEDGMENT

The work described here was performed in part at the LLE National Laser Users' Facility (NLUF) and was supported in part by U.S. DOE (Grant No. DE-FG03-03SF22691), LLNL (subcontract Grant No. B504974), and LLE (subcontract Grant No. 412160-001G).

REFERENCES

1. B. B. Kadomstev, in *Reviews of Plasma Physics*, edited by M. A. Leontovich (Consultants Bureau, New York, 1966), Vol. 2, pp. 153–199.
2. J. P. Freidberg, *Ideal Magnetohydrodynamics* (Plenum Press, New York, NY, 1987).
3. W. Baumjohann and R. A. Treumann, *Basic Space Plasma Physics* (Imperial College Press, London, 1996).
4. S. Eliezer, *The Interaction of High-Power Lasers with Plasmas* (Institute of Physics Publishing, Bristol, England, 2002).
5. M. G. Haines, Phys. Rev. Lett. **78**, 254 (1997).
6. S. I. Braginskii, in *Reviews of Plasma Physics*, edited by Acad. M. A. Leontovich (Consultants Bureau, New York, 1965), Vol. 1, p. 205.
7. J. A. Stamper *et al*., Phys. Rev. Lett. **26**, 1012 (1971); D. G. Colombant and N. K. Winsor, Phys. Rev. Lett. **38**, 697 (1977); A. Raven, O. Willi, and P. T. Rumsby, Phys. Rev. Lett. **41**, 554 (1978); M. Borghesi *et al*., Phys. Rev. Lett. **81**, 112 (1998); A. J. Mackinnon, P. K. Patel, R. P. Town, M. J. Edwards, T. Phillips, S. C. Lerner, D. W. Price, D. Hicks, M. H. Key, S. Hatchett, S. C. Wilks, M. Borghesi, L. Romagnani, S. Kar, T. Toncian, G. Pretzler, O. Willi, M. Koenig, E. Martinolli, S. Lepape, A. Benuzzi-Mounaix, P. Audebert, J. C. Gauthier, J. King, R. Snavely, R. R. Freeman, and T. Boehly, Rev. Sci. Instrum. **75**, 3531 (2004); U. Wagner *et al*., Phys. Rev. E **70**, 026401 (2004).
8. M. G. Drouet and R. Bolton, Phys. Rev. Lett. **36**, 591 (1976); M. A. Yates *et al*., Phys. Rev. Lett. **49**, 1702 (1982).
9. C. K. Li, F. H. Séguin, J. A. Frenje, J. R. Rygg, R. D. Petrasso, R. P. J. Town, P. A. Amendt, S. P. Hatchett, O. L. Landen, A. J. Mackinnon, P. K. Patel, V. A. Smalyuk, T. C. Sangster, and J. P. Knauer, Phys. Rev. Lett. **97**, 135003 (2006).
10. M. G. Haines, Phys. Rev. Lett. **47**, 917 (1981).
11. R. P. J. Town *et al*., Bull. Am. Phys. Soc. **51**, 142 (2006).
12. G. B. Zimmerman and W. L. Kruer, Comments Plasma Phys. Control. Fusion **2**, 51 (1975).
13. P. D. Nielsen and G. B. Zimmerman, Lawrence Livermore National Laboratory, Livermore, CA, UCRL-53123 (1981).
14. D. R. Welch *et al*., Nucl. Instrum. Methods Phys. Res. A **464**, 134 (2001).
15. T. R. Boehly, D. L. Brown, R. S. Craxton, R. L. Keck, J. P. Knauer, J. H. Kelly, T. J. Kessler, S. A. Kumpan, S. J. Loucks, S. A. Letzring, F. J. Marshall, R. L. McCrory, S. F. B. Morse, W. Seka, J. M. Soures, and C. P. Verdon, Opt. Commun. **133**, 495 (1997).
16. T. J. Kessler, Y. Lin, J. J. Armstrong, and B. Velazquez, in *Laser Coherence Control: Technology and Applications*, edited by H. T. Powell and T. J. Kessler (SPIE, Bellingham, WA, 1993), Vol. 1870, pp. 95–104.
17. C. K. Li, F. H. Séguin, J. A. Frenje, J. R. Rygg, R. D. Petrasso, R. P. J. Town, P. A. Amendt, S. P. Hatchett, O. L. Landen, A. J. Mackinnon, P. K. Patel, V. Smalyuk, J. P. Knauer, T. C. Sangster, and C. Stoeckl, Rev. Sci. Instrum. **77**, 10E725 (2006).
18. F. H. Séguin, J. L. DeCiantis, J. A. Frenje, S. Kurebayashi, C. K. Li, J. R. Rygg, C. Chen, V. Berube, B. E. Schwartz, R. D. Petrasso, V. A. Smalyuk, F. J. Marshall, J. P. Knauer, J. A. Delettrez, P. W. McKenty, D. D. Meyerhofer, S. Roberts, T. C. Sangster, K. Mikaelian, and H. S. Park, Rev. Sci. Instrum. **75**, 3520 (2004).
19. W. L. Kruer, *The Physics of Laser Plasma Interactions* (Westview Press, Boulder, CO, 2003).